# IMPACT OF LBM PROCESS DEFECTS ON MECHANICAL PROPERTIES OF AS7G06 ALUMINIUM ALLOY

Olivier Quénard, Philippe Guy, Olivier Dorival, Arnaud Votié, Sébastien Begoc

# IMPACT OF LBM PROCESS DEFECTS ON MECHANICAL PROPERTIES OF AS7G06 ALUMINIUM ALLOY

**O. Quénard [(1)], Ph. Guy [(1)], O. Dorival [(1,2)], A. Votié [(3)], S. Begoc [(4)],**

*[(1)] Icam, 75 avenue de Grande-Bretagne, 31300 Toulouse, France, +33 (0)5 34 50 50 36, olivier.quenard@icam.fr and philippe.guy@icam.fr*
*[(2)] Université de Toulouse ; Institut Clément Ader UMR CNRS 5312, INSA/UPS/ISAE/Mines Albi, 3 rue Caroline Aigle F-31400 Toulouse, France, +33 (0)5 34 50 50 55, olivier.dorival@icam.fr*
*[(3)] FusiA, 8 rue Claude Gonin 31400 Toulouse, France, +33 (0)5 62 80 21 10, a.votie@fusia.fr*
*[(4)] Cnes, 18 av. Edouard Belin 31401 Toulouse, France, +33 (0)5 61 27 43 75, sebastien.begoc@cnes.fr*

## ABSTRACT

This paper deals with the influence of the size of defects on the mechanical properties of AS7G06 samples manufactured by Laser Beam Melting (LBM). Among all the potential defects that could appear in the samples, porosity is the only one that can be created during the manufacturing process by mastering both size and orientation. The results reveal that, on the stress-relieved samples, the porosity has no influence on the measured tensile mechanical properties, even when representing 3.5% of the cross section area, but for elongation at break which strongly decreases when increasing the size of the defect.

## 1. INTRODUCTION

For a few decades, additive manufacturing (AM) appeared as on the way of revolutionizing both the design possibilities and the manufacturing standards. It is now used as a regular technique in space and aircraft industry. Design limits were incredibly stretched thank to unprecedented freedom and part complexity. Moreover, AM totally fits the use of CAD tools, thus matching topology (and weight) optimization approach well. Global manufacturing time and cost were deeply changed due to the decrease in the number of processing operations and number of parts. Additionally, AM leads to an optimal use of raw material.

Nevertheless, the use of AM parts can be limited in some fields of application by the presence of defects in the material, which can accelerate the initiation of fracture of the sample and/or reduce its mechanical properties.

Many papers can be found in literature about the process-microstructure-tensile property relations for the LBM process [1-5]. Several studies deal with the origin of the defects, mostly the porosity which is the more frequently obtained defect [6-11]. Gong et al. [11] studied the influence of both scanning rate and laser power on the porosity rate, as well as the shape of the resulting pores. They also demonstrated that the average size of the pores increases with the porosity rate [12]. But none of these studies is related to the influence of defect on the mechanical properties of the obtained LBM samples.

The present contribution deals with the influence of pore on the tensile properties of AS7G06 samples.

## 2. SAMPLES PREPARATION AND TESTING METHODS

### 2.1 Manufacturing

All the samples have been manufactured with an EOS M280 machine using a 1060-1100 µm wavelength laser. Layers were 60 µm thick. Building orientation z is vertical. The AS7G06 powder is provided by Advanced Powders and Coatings, with 15-45 µm particle size. The powder has been recycled less than 15 times. Two batches have been manufactured on a building platform heated, with the same parameters. The only difference between the two batches concerns the temperature of this building platform: 200°C for batch #1 and 170°C for batch #2. This in-situ heating allows relieving thermal stresses due to LBM process. No further heat treatment has been performed, all the study is focused on the stress-relieved samples.

In order to determine the obtained size and shape of the pores (vs the expected size and shape) after LBM manufacturing, two samples, called "technological samples", have been prepared (batch #1). The process parameters have been encoded in order to obtain pores of various height and orientation. These pores are in each case of square morphology. This square can be either perpendicular or slanted (45°) with reference to the z axis. Whatever the orientation, the theoretical dimension of the projected area on a plan perpendicular to the z axis is 1 mm². The height of the pores is ranging between 60 and 840 µm, with 60 µm steps (Figure 1).

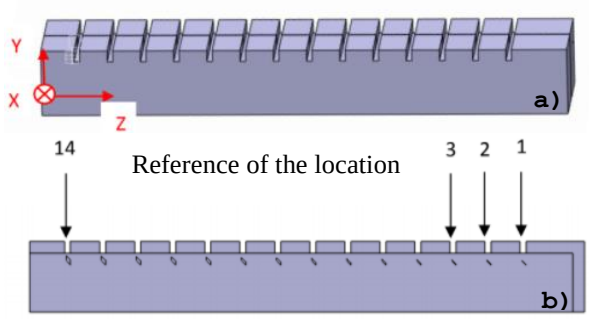


*Figure 1. Design of Technological Sample (a) - Cross Section showing the Different Size Slanted Defects (b)*

The samples for tensile test (batch #2) were rods, the diameter of which was 10 mm, manufactured along the z direction. After LBM process, machining (mostly by

turning) led to specimens with the expected surface quality and with dimensions in agreement with that specified by ASTM E8 norm [13]: standard round specimen, diameter for the section: 6 mm, length of the reduced section: 27 mm, total length: 60 mm.

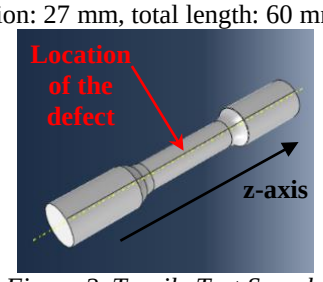


*Figure 2. Tensile Test Sample*

Seven series of samples have been manufactured. The first one was composed of specimen without any expected porosity (called "reference" in the following). For the six other series, the centre of the reduced section of each specimen was expected to present one square pore, the height of which is 600 µm. Depending on the series, the dimensions of the projected square are expected to be 100x100 µm², 500x500 µm² and 1 000x1 000 µm². For a sake of brevity, these three dimensions will be call "100 µm", "500 µm" and "1 000 µm" respectively in the following. These three dimensions for each of the 2 orientations (perpendicular and slanted) led to 6 series of specimens.
For the sake of a representative statistical analysis, each series was composed of 7 samples.

### 2.2 Mechanical Testing

Tensile tests were performed on a Instron electro-mechanical testing machine of type UTM-EM equipped with wedge grips. Machine driving was performed by Bluehill 2.21 software. A 2525-801 type 100 kN Instron load cell was used to record the tensile force. A 12.5mm 2620-601 Instron clip-on extensometer was used to measure the axial strain of the specimen. Tests were performed according to recommendation of norms ASTM E8 [13] and NF EN 10002-1 [14]. Stress rate of 2 MPa/s was used till reaching 90 MPa. Then strain rate of 0.00025 $s^{-1}$ was prescribed. At 3.5% strain, the clip-on extensometer was removed manually, and strains were measured directly by the crosshead displacement. The yield strength is determined by the usual offset method (offset = 0.2%).
For stress calculation (both yield stress and mechanical resistance), the diameter of the cross section is measured at three different locations along the calibrated length of each specimen using a micrometer in order to obtained a representative average value.

### 2.3 Optical and SEM observations

Optical observations were performed with a ZEISS Axiotech microscope (magnification ranging between x5 to x100), a PRESIVIEW software allowing acquiring images. For larger magnification (up to x10 000), a HITACHI TM1000 scanning electron microscope (SEM) was available.

## 3. RESULTS

### 3.1 Technological Samples (Batch #1)

Optical observations were performed on each of the technological samples, after polishing until reaching the pores in the centre of the specimens. The aim of such observations was to measure the dimensions (mostly the height) of the pores and to compare them to the theoretical ones. Table 1 shows the results in the case of sample containing pores perpendicular to the z-axis. The positions of the pores, described in Fig. 1, allow remembering the theoretical height of the defect.
One can note that no defect can be detected for pores which theoretical height is no higher than 240 µm. That means that the laser beam scanning melts a depth of solid material equivalent to at least 4 times the thickness of a layer of powder (60 µm). This value of re-melted depth is not confirmed by the values obtained for the largest defects. Indeed, the difference in height is mostly ranging between 130 and 190 µm, representing between 2 and 3 times the thickness of a layer of powder.
Optical observations revealed also that the shape and width of the pores is close to the expected ones (rectangular with width close to 1 mm, Fig. 3-a) for the largest pores (at least 480 µm of theoretical height). Nevertheless, for the smallest ones, it appears that the pore is not a single cavity, but rather a series a small pores (Fig. 3-b).
These results have been confirmed by tomographic analysis performed by CNES. Indeed, the largest ones reveal the expected shape and width (Fig. 4-a), even if the height is lower than the theoretical one, while only a cloud of very small pores can be detected for the smallest theoretical defects (Fig. 4-b). Small unexpected pores, the size of which is difficult to evaluate (some micrometers) have also been detected.

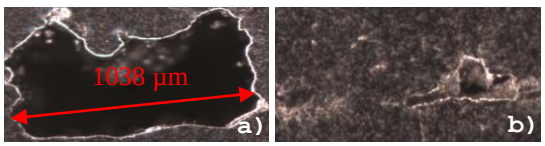


*Figure 3. Shape of the Pores depending on the Theoretical Height: 780 µm (a) and 300 µm (b)*

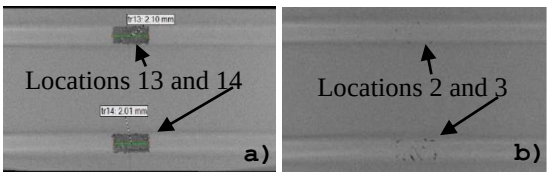


*Figure 4. Tomographic Detection of the Defect for Large Theoretical Defects (a) and Small Ones (b)*

Quite similar results were obtained with the technological sample presenting slanted pores (Table 2). Indeed, it appears that the height of the defect is lower than the expected ones, what can be of course attributed to the re-melting of the previous layers by the laser beam during the manufacturing. Nevertheless, two differences must be underlined. On the one hand, only the first two positions did not reveal any porosity,

meaning that the re-melting in this case seems to affects only 2 layers. But this result in not confirmed by the values obtained for the largest defects. Indeed, and this is the second difference, the proportional variation seems to increase with the theoretical height of the pores, reaching a loss of 53% of height for location 11.
Optical observations revealed that the shape of the defects is hardly homogeneous. If the slant angle is correct (45°), the opposite faces of the pores are hardly plane and parallel (Fig. 5). Depending on the samples, the extreme angles of the pores can be either obtuse (almost circular, Fig. 5-a) or acute (Fig. 5-b). This difference can lead to much different local stress concentration when performing tensile tests.

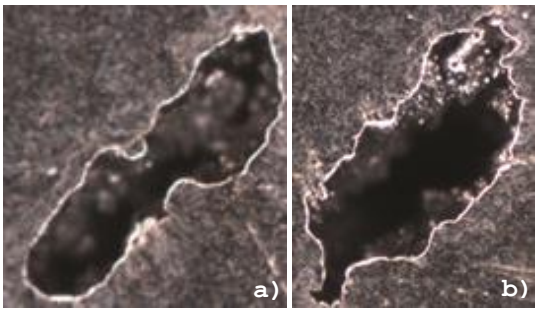

*Figure 5. Obtuse Angle (a) and Acute Angle (b) for 360 µm and 720 µm Theoretical Height Pores respectively*

All of these results have been confirmed by tomography analysis performed by Cnes.

| **reference of the defect** | **1 to 4** | **5** | **6** | **7** | **8** | **9** | **10** | **11** | **12** | **13** | **14** |
|---|---|---|---|---|---|---|---|---|---|---|---|
| **Theoretical height (µm)** | 60 to 240 | 300 | 360 | 420 | 480 | 540 | 600 | 660 | 720 | 780 | 840 |
| **Measured height (µm)** | 0 | 142 | 229 | 229 | 332 | 551 | 468 | 489 | 529 | 657 | 749 |
| **Absolute variation (µm)** | < 240 | 158 | 131 | 191 | 148 | 11 | 132 | 171 | 191 | 123 | 91 |
| **Proportional variation (%)** | 0 | -53 | -36 | -45 | -31 | 2 | -22 | -26 | -27 | -16 | -11 |

*Table 1. Comparison between Theoretical and Measured Height of the Pores Perpendicular to the z-Axis in the First Technological Sample*

| **reference of the defect** | **1 to 2** | **3** | **4** | **5** | **6** | **7** | **8** | **9** | **10** | **11** | **12** | **13** | **14** |
|---|---|---|---|---|---|---|---|---|---|---|---|---|---|
| **Theoretical height (µm)** | 60 to 120 | 180 | 240 | 300 | 360 | 420 | 480 | 540 | 600 | 660 | 720 | 780 | 840 |
| **Measured height (µm)** | 0 | 160 | 160 | 240 | 250 | 362 | 345 | 366 | 445 | 430 | 426 | 523 | 584 |
| **Absolute variation (µm)** | 0 | 20 | 80 | 60 | 110 | 58 | 135 | 174 | 155 | 230 | 294 | 257 | 256 |
| **Proportional variation (%)** | 0 | -11 | -33 | -20 | -31 | -14 | -28 | -32 | -26 | -53 | -41 | -33 | -44 |

*Table 2. Comparison between Theoretical and Measured Height of the Slanted Pores (45° with reference to the z-Axis) in the Second Technological Sample*

### 3.2 Mechanical Results (Batch #2)

Measurement results are presented in terms of average values (6 to 7 samples in each series) with the associated standard deviation (Table 3). One must note that in all cases, the fracture occurred within the calibrated length of the specimen.

In order to determine the influence of the size of a pore, or the orientation of the defect, in a stress-relieved AS7G06 specimen, one must compare the obtained values of Young Modulus (E), Tensile Yield Stress (TYS, or $R_{p0.2}$) , Ultimate Tensile Stress (UTS, or $R_m$) and Elongation at Break (A) to that of the reference (specimen without expected porosity).

If the mechanical properties of AS7G06 in a T6 state are quite easy to find in literature, that of stress-relieved AS7G06 without any post-treatment are hardly presented. So, it seems to be difficult to evaluate if these properties in our study are high or not for such an alloy.

When comparing, the obtained values for the specimen with pores seems to be very close to that of the reference whatever the size of the defect.

The Young Modulus is ranging between 71.6 and 72.7 MPa for all the samples but that with the 1 000 µm slanted defect. Indeed, in this later case, the Modulus is decreased down to 69.9 MPa. Nevertheless, the variation in comparison to the reference (-1.9 MPa) is of the same order as the standard deviation (1.5 and 2.9 MPa for the reference and the studied specimen respectively), meaning that it is not representative.

Similar comments can be done concerning the stresses (TYS and UTS).

The only correlation that could be done for these three characteristics is the increase in the standard deviation of the Young Modulus with the increase in size of the defect, whatever the orientation of this latter.

When comparing the Elongation at Break, it quickly appears that it keeps almost constant when the size of the defect is not higher than 500 µm. But it suddenly strongly decreases when the size reaches 1 000 µm.

| | Kind of Defect | | Young's Modulus E (GPa) | Tensile Yield Strength $R_{p0,2}$ (MPa) | Ultimate Tensile Strength $R_m$ (MPa) | Elongation at break A (%) | Number of Samples |
|---|---|---|---|---|---|---|---|
| | Orientation | Size | | | | | |
| Ref. | / | / | 71,8 ± 1,5 | 193 ± 2 | 335 ± 2 | 7,0 ± 0,3 | 6 |
| Defects | Perpendicular | 100 µm | 72,8 ± 2,4 | 201 ± 5 | 343 ± 3 | 6,7 ± 0,5 | 7 |
| | | 500 µm | 71,6 ± 3,0 | 195 ± 4 | 335 ± 1 | 6,5 ± 0,4 | 6 |
| | | 1000 µm | 71,8 ± 3,7 | 200 ± 6 | 338 ± 6 | 4,1 ± 0,2 | 7 |
| | Slanted | 100 µm | 71,9 ± 1,3 | 207 ± 15 | 341 ± 2 | 6,8 ± 1,1 | 6 |
| | | 500 µm | 72,7 ± 2,0 | 196 ± 7 | 339 ± 7 | 6,1 ± 0,1 | 7 |
| | | 1000 µm | 69,9 ± 2,9 | 192 ± 5 | 329 ± 2 | 4,2 ± 0,4 | 7 |

*Table 3. Mechanical Properties of LBM AS7G06 Specimens built with Different Defects*

For a better understanding, instead of presenting only the raw data, we thought that it could be interesting to analyse the evolution of each characteristic in terms of proportion, compared to that of the reference. Table 4 presents these variations calculated by dividing the difference between the characteristic of a given kind of specimen and the reference by the value obtained for the reference.

Of course, the influence of the size of a given defect is also dependant on the cross section of the specimen. That's why we also calculated the cross section area (CSA) of the specimens, the projected surface area of the defect (DPA), and of course, the CSA-to-DPA ratio (Table 4).

This analyse confirms that, if the variations in E, $R_{p0.2}$ and $R_m$ are negligible (and in every case lower than the CAS-to-DPA ratio), the elongation at break strongly decreases when increasing the dimensions of the defect. Indeed, a pore (the size of which is 500 µm) representing less than 1% of the cross section of the sample leads to 7 to 13% of elongation loss, and when representing 3.5% of the cross section (1 000 µm in size), the loss reaches around 40% of the elongation at break.

This behaviour reveals that the specimen tends to be less ductile, and on the opposite more brittle, when the size of the defect increases.

| | Kind of Defect | | Relative Variation (%) | | | | Cross-Sectional Area (mm²) | Defect Projected Area (mm²) | CSA-to-DPA Ratio |
|---|---|---|---|---|---|---|---|---|---|
| | Orientation | Size | $\Delta E / E_{ref.}$ | $\Delta R_{p0,2} / R_{p0,2\,ref.}$ | $\Delta R_m / R_{m\,ref.}$ | $\Delta A / A_{ref}$ | | | |
| Ref. | / | / | 71,8 GPa | 193 MPa | 335 MPa | 7,0% | 28,23 | / | / |
| Defects | Perpendicular | 100 µm | 1,4% | 4,1% | 2,4% | -4,3% | 28,15 | 0,010 | 0,036% |
| | | 500 µm | -0,3% | 1,0% | 0,0% | -7,1% | 28,31 | 0,250 | 0,883% |
| | | 1000 µm | 0,0% | 3,6% | 0,9% | -41,4% | 28,18 | 1,000 | 3,549% |
| | Slanted | 100 µm | 0,1% | 7,3% | 1,8% | -2,9% | 28,35 | 0,010 | 0,035% |
| | | 500 µm | 1,3% | 1,6% | 1,2% | -12,9% | 28,46 | 0,250 | 0,878% |
| | | 1000 µm | -2,6% | -0,5% | -1,8% | -40,0% | 28,14 | 1,000 | 3,554% |

*Table 4. Influence of Defects on the Mechanical Properties (in terms of Average Relative Variation)*

Optical observation of the fractured samples allows having first indications.

Indeed, as the reference presents an expected homogeneous reduced section, the fracture occurs statistically anywhere (Fig. 6-a).

For the samples containing defects, it was expected that the fracture occurs strictly in the middle of the reduced sample, where the defect is located (Fig. 2). Nevertheless, for the 100 and 500 µm defects, the fracture does not occur where expected, but statistically anywhere (Fig. 6-b), like for the reference. This observation reveals that the pore of such sizes (or which CSA-to-DPA ratio is lower than 1%) does not weaken the corresponding specimens. On the opposite, for the sample containing a 1 000 µm pore, the fracture occurs exactly in the middle of the specimen, where the pore is located. The defect is easily detectable on the fracture surface (Fig. 6-c). These observations allow understanding why the mechanical properties of the samples are independent of the size of the defects as long as they represent less than 1% of the cross section area.

Nevertheless, these optical analyses do not allow explaining the loss of elongation at break.

In order to analyse more deeply the behaviour of our samples, and the influence of the size of pores, we observed the fracture surface of the samples by SEM.


*Figure 6. Optical Observation of the Fracture Surface of the Reference (a), and Samples Containing 500 µm (b) and 1 000 µm Pore (c)*

SEM observations of the fracture surface of the reference reveals two kinds of behaviours (Fig. 6). In the centre part of the surface, the sample appears to be largely ductile, owing to the large network of cups that can be observed. One can note also quite linear smooth dimples, which are attributed to interlayer fracture. This conclusion is supported by the fact that orientation of the various dimples create an angle attributed to the change in angle when scanning from layer to layer during the manufacturing. Such a behaviour has already been observed for other metallic samples [5].

On the edge, the ductile behaviour seems to decrease, the smooth fracture surfaces indicating that the behaviour becomes more and more brittle. This global fracture behaviour is typical of a ductile sample: when submitted to tensile stress, the fracture occurs in the centre of the specimen, by formation of micro-porosity (detectable in Fig. 6). Once these micro-pores coalesced, the residual section of the specimen is largely decreased, inducing a faster fracture in the peripheral section, leading to this "more brittle" aspect.

The fracture surface of the specimen containing pores of 100 and 500 µm size are largely similar to that of the reference.

When observing the fracture surface of specimens containing pore of 1 000 µm size, the defect is immediately detectable in the centre of the section (Fig. 7). Measurement of the defect confirms that its size is conformed to the expected one (1 000 x 1 000 µm²). The walls of the pore present many partially melted particles of alloy (most of the particles embedded in the pore are unmelted and escape when the sample breaks).

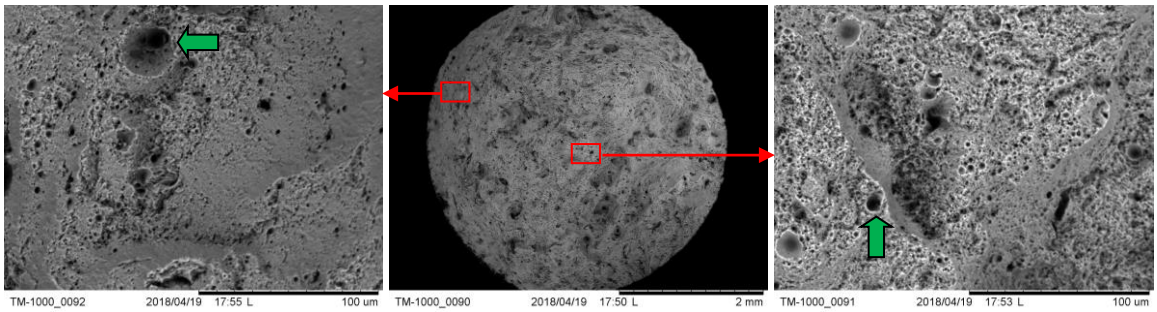


*Figure 6. Fracture Surface of the Reference at Different Magnifications (x40: middle; x300: left and right) and Different Locations (Peripheral Area: left; Centre Area: right)*

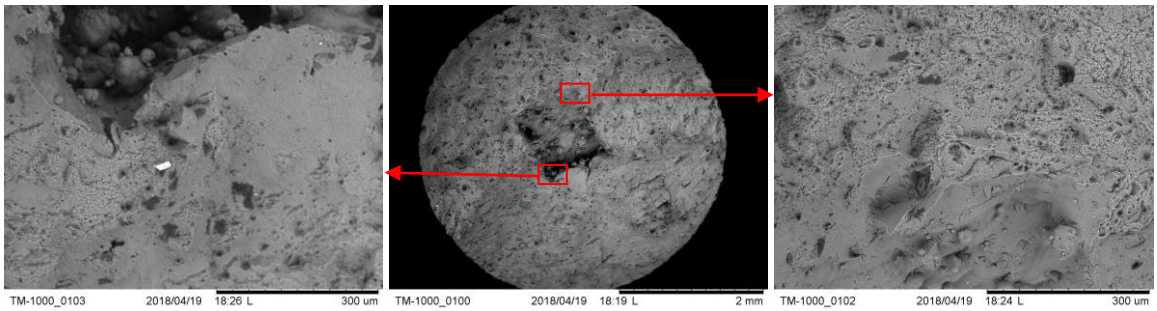


*Figure 7. Fracture Surface of a Specimen Containing a Slanted Pore, the Size of which is 1000x1000 µm² (centre) - Higher Magnification Revealing a Brittle Behaviour (x300: left) and Ductile Behaviour (x300: right)*

It is clear that, if a large proportion of the fracture surface exhibits a ductile behaviour (Fig. 7 – right), a significant proportion reveals on the opposite a much more brittle behaviour (Fig. 7 – left), even in the centre of the section. The edge of the section also exhibits a mixed ductile-brittle behaviour, similar to that of the

reference (Fig. 8). Once again, a network of dimples reveals an interlayer fracture.

These observations, revealing a larger proportion of surface area submitted to brittle behaviour, allow explaining why the specimen containing large pores (1 000 µm, representing 3.5% of the cross section area) present a strong decrease in their elongation at break.

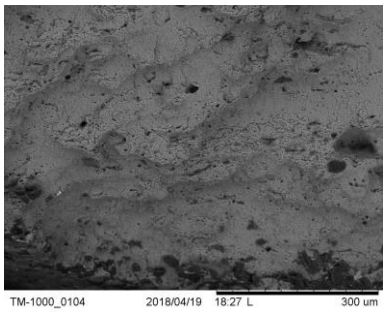


*Figure 9. Fracture Surface on the Edge of a Specimen Containing a 1 000 µm Pore*

## 4. CONCLUSION

This study reveals that the pores in stress-relieved AS7G06 parts produced by LBM process are of low influence on the mechanical performances as long as the size does not represent more than 3.5% of the cross section area of the part, elongation at break quickly falls down when increasing the size of the pore.

Nevertheless, these results are only the first step in the determination of the influence of porosity on mechanical properties of AS7G06 parts produced by LBM. Indeed, the stress-relieved state is not the standard state of this alloy. So, it seems that influence of post heat-treatment (T6, CIC) must be studied also. Further works are in progress in such a way.

**Aknowledgements:** The authors wish to acknowledge Centre National des Etudes Spatiales (Cnes) for support through Grant no. 161516/00, the tomographic analysis and implication during the recurrent informal meetings. We also thank FusiA company for providing the stress-relieved manufactured samples.

Our acknowledgements also to Thales Alenia Space for the technical discussions we regularly have.

## REFERENCES

1. Thijs, L., Verhaeghe, F., Craeghs, T., Van Humbeeck, J., Kruth, J.-P. (2010). A study of the microstructural evolution during selective laser melting of Ti-6Al-4V, *Acta Mater*, **58**, 3303-3312.
2. Facchini, L., Magalini, E., Robotti, P., Molinari, A., Höges, S., Wissenbach, K. (2010). Ductility of a Ti-6Al-4V alloy produced by selective laser melting of prealloyed powders, *Rapid Prototyping Journal*, **16**(6), 450-459.
3. Vrancken, B., Thijs, L., Kruth, J.-P., Van Humbeeck, J. (2012). Heat treatment of Ti6Al4V produced by Selective Laser Melting: microstructure and mechanical properties, *Journal of Alloys and Compounds*, **541**, 177-185.
4. Quénard, O., Dorival, O., Guy, Ph., Votié, A., Brethome, K. (2018). Measurement of fracture toughness of metallic materials produced by additive, *CEAS Journal* (in press).
5. Quénard, O., Dorival, O., Guy, Ph., Brethome, K. (22-25 February 2018). Measurement of residual stresses and toughness in Ti-6Al-4V material produced by laser beam Manufacturing, *Proceedings of the IC4M, International Conference on Mechanical, Manufacturing, Modeling and Mechatronics* (Barcelona, Spain).
6. Kruth, J.-P., Badrossamay, M., Yasa, E., Deckers, J., Thijs, L., Van Humbeeck, J. (2010). Part and material properties in selective laser melting of metals, *Catholic University of Leuven*, 12.
7. Yan, M., Yu, P. (2015). An Overview of Densification, Microstructure and Mechanical Property of Additively Manufactured Ti-6Al-4V - Comparison among Selective Laser Melting, Electron Beam Melting, Laser Metal Deposition and Selective Laser Sintering, and with Conventional Powder Metallurgy, *Sintering Techniques of Materials*, ISBN 978-953-51-2033-9.
8. Sames, W. J., List, F. A., Pannala, S., Dehoff, R. R., Babu, S. S. (2016). The metallurgy and processing science of metal additive manufacturing, *International Materials Reviews*, 0950-6608.
9. Aboulkhair, N. T., (2016). Additive manufacture of an aluminium alloy: processing, microstructure, and mechanical properties, *University of Nottingham*, 293.
10. Aboulkhair, N. T., Everitt, N. M., Ashcroft, I., Tuck, C. (2014). Reducing porosity in AlSi10Mg parts processed by selective laser melting, *University of Nottingham, Additive Manufacturing*, **1**(4), 77–86.
11. Gong, H., Rafi, K., Starr, T., Stucker, B. (2013). The Effects of Processing Parameters on Defect Regularity in Ti-6Al-4V Parts Fabricated By Selective Laser Melting and Electron Beam Melting, *University of Louisville*, 17.
12. Gong, H., Rafi, K., Gu, N.V., Starr, T., Stucker, B. (2013). Defect Morphology in Ti-6Al-4V Parts Fabricated By Selective Laser Melting and Electron Beam Melting, J.B Speed School of Engineering, 440-453.
13. ASTM E8 / E8M-15a, (2015). Standard Test Methods for Tension Testing of Metallic Materials, *ASTM International*, West Conshohocken, PA, www.astm.org.
14. .NF EN 10002-1, (2001). Matériaux métalliques - Essai de traction - Partie 1 : méthode d'essai (à la température ambiante), *AFNOR*, www.afnor.org.